Vibrational dynamics of amorphous ice structures studied by high-resolution neutron spectroscopy

Michael Marek Koza*
Institut Laue Langevin, 6 Rue Jules Horowitz, Boite Postale 156, 38042 Grenoble, Cedex 9, France
(Received 14 April 2008; published 18 August 2008)

The dynamics of amorphous water ice structures of different densities have been studied by high-resolution neutron time-of-flight and backscattering spectroscopy. An accurate determination of the vibrational density of states $G(\omega)$ in the energy range of phonons $\hbar\omega \lesssim 40$ meV of a many fold of structures comprising the low-density amorphous (LDA, $\rho \approx 31$ molecules/nm^3), high-density amorphous (HDA, $\rho \approx 39$ molecules/nm^3), very-high-density amorphous (vHDA, $\rho \approx 41$ molecules/nm^3) and modifications of intermediate density in respect to HDA and vHDA has been achieved. Unlike the $G(\omega)$ of high-density crystalline phases IX, V, and XII, which have been measured as reference systems, the $G(\omega)$ of all high-density amorphous counterparts proves to be textureless except for a predominant peak at low energies. In vHDA this peak is centered at about 10 meV and redshifted upon density decrease to 7 meV in LDA. A concomitant upshift of the low-energy librational band edge from 34 to 45 meV is detected in deuterated samples. Mean-square displacement and Debye temperatures T_D for vHDA, HDA′—a structure obtained as a transient product of the temperature induced vHDA to LDA transformation—and LDA are extracted from the highest resolution backscattering experiments. T_D values indicate the absence of a dominant excess of low-energy modes in $G(\omega)$, referred to as boson peak in the literature, being in agreement with the $G(\omega)$ properties directly monitored by the time-of-flight technique. Having applied deuterated sample material we are able to display phase coherence effects within the phonon system in the second and third pseudo-Brillouin zone ($1\ \text{Å}^{-1} \leq Q \leq 5\ \text{Å}^{-1}$) of the amorphous samples. A phase coherent signal from acoustic phonons can be followed up to energies of at least 15 meV.

DOI: 10.1103/PhysRevB.78.064303 PACS number(s): 63.50.Lm, 61.43.−j, 61.05.fg, 64.70.Ja

I. INTRODUCTION

The collective translational dynamics (phonons) of amorphous water ice structures display features which are extraordinary for inelastic properties of disordered systems. It has been shown by inelastic x–ray scattering (IXS) experiments that the acoustic phonon branches are well defined in a wide range of the energy–momentum ($\hbar\omega - Q$) phase space.[1,2] A remarkably narrow line width of the longitudinal acoustic mode indicates long phonon lifetime and, hence, a long mean free path. Phonon selection rules are at work governing the intensity of the signal in scattering experiments and pointing at unexpectedly well-defined eigenvectors of transverse and longitudinal acoustic and optic character for a disordered system. A qualitative comparison with the dynamic structure factor of crystalline phases revealed a similar response of the low-density amorphous (LDA,[3] $\rho \approx 31$ molecules/nm^3) modification with that of crystalline cubic ice I_c ($\rho \approx 31$ molecules/nm^3) and of the high-density amorphous (HDA,[3] $\rho \approx 39$ molecules/nm^3) with the response of high-density crystalline ice IX[4,5] ($\rho \approx 39$ molecules/nm^3, $P4_12_12$) and ice XII[6,7] ($\rho \approx 43$ molecules/nm^3, $I\bar{4}2d$).

Results from inelastic neutron scattering (INS) experiments showed that they are in agreement with the crystal-like dynamics established by IXS. For example, no strong excess of phonon modes was found in LDA when compared to ice I_c and the crystalline hexagonal modification ice I_h.[8–11] Such a mode excess is a characteristic feature of disordered systems in particular of strong glasses to which LDA is supposed to belong.[12,13] This excess is often termed boson peak as the excitations follow the thermal occupation of a Bose system, i.e., phonons. For HDA high-resolution backscattering experiments revealed a Debye temperature T_D tending to exceed the one of the polycrystalline ice I_c supporting the conclusion of the absence of a boson peak when compared to ice I_c and I_h.[9,11]

Parameters and properties which could be extracted and conjectured from the microscopic dynamics monitored by INS and IXS proved to be in good agreement with macroscopic results, which are linked to the samples' acoustic phonons and can be measured by different techniques. For example, this agreement comprises velocity of sound values and, hence, T_D probed by ultrasonic experiments,[14,15] as well as thermal conductivity studies revealing a crystal-like behavior for LDA.[16,17]

Another unique feature of the dynamics of amorphous ice structures and a remarkable analogy between macroscopic and microscopic observables has been recently established upon pressure-induced transformations. It was shown that LDA, like its crystalline counterparts ice I_c and I_h but unlike HDA, exhibits negative Grueneisen and Bridgman parameters,[18] an observation being in line with the conclusion from ultrasonic experiments that both pressure-induced transformations from I_h to HDA and from LDA to HDA are due to elastic instability.[14,19–21] The microscopic correspondence is found again by INS measurements[22,23] as a mechanical melting process.[24–26] Consequently, the entire body of experimental results on dynamic and thermodynamic properties of amorphous and crystalline structures sets a huge question mark on the discussion of thermodynamics being responsible for the existence of amorphous structures of different density and of phase transitions between them.[27,28]

So far, the experimental work has been strongly focused on the microscopic dynamics of LDA and HDA and only few

TABLE I. Sample designation according to the nominal annealing temperature T_{an} and annealing pressure p_{an}. Please note that sample 7 was first heated to 120 K before having been compressed to 1.5 GPa. All other samples were first compressed at 77 K before having applied T_{an}. Spectrometers utilized for the study are indicated at the bottom.

	1	2	3	4	5	6	7	8	9	10
T_{an}/K	77	100	120	140	150	140	120	140	140	77
p_{an}/GPa	1.5	1.5	1.5	1.5	1.5	1.2	1.5	1.5	1.5	1.5
spectr.	IN6	IN6	IN6	IN6	IN6	IN6	IN6	IN4	IN13	IN13

information is available on the inelastic response of the very-high-density amorphous structure (vHDA,[24,29,30] $\rho \approx 41$ molecules/nm^3). Since vHDA, like LDA and in contrast to HDA, appears to be a homogeneously disordered structure,[31–34] we might expect the inelastic response to reflect dynamic properties detected with HDA in an even more distinguished way. We aim with the present study at the establishment of the vibrational density of states of different high-density amorphous ice structures with best energy resolution, and at the inspection of dispersion properties of collective modes as they can be sampled by coherent inelastic neutron scattering (CINS).

This paper is structured as follows. We begin with an introduction to the sample preparation, to the applied neutron spectrometers, and to the experimental procedure. We continue with the results which comprise a general presentation of coherence effects in the scattering signal, a detailed discussion of the generalized vibrational density of states $G(\omega)$, and a presentation of the mean-square displacements and of the Debye temperatures as they can be determined from highest resolution backscattering experiments. A comparison of $G(\omega)$ with results on high-density crystalline structures IX, V, and XII measured as reference systems is presented. This chapter is finished by a detailed discussion of phase coherence properties and dispersing acoustic modes monitored by CINS before in a detailed discussion chapter a link of the results is made to literature data. We finalize this manuscript with a summary of the most important results.

II. EXPERIMENT

Details of the sample preparation are given in Ref. 32. Note that the samples we refer to in the present paper as 1–7 are moieties from the very samples studied by diffraction and small-angle scattering techniques in Refs. 32 and 34. Their inelastic response has been measured exclusively at the cold time-of-flight spectrometer IN6@ILL. In addition we have measured three other samples. Two deuterated (D_2O, purity of 99.8%) very-high density structures having followed the preparation recipe of sample 4 and a fully protonated (H_2O, millipore grade) high-density amorphous structure. An overview of the sample preparation conditions and spectrometers applied is given in Table I.

In addition we have prepared and measured three high-density crystalline samples ice IX, V, and XII. These samples were prepared by compression of hexagonal ice at appropriate temperatures. Ice XII was prepared at 77 K and rapid compression to 1.8 GPa.[35,36] Ice IX was prepared at about 170–180 K and maximum applied pressure of 1.0 GPa.[4,35] Ice V was obtained at 240–245 K at a nominal pressure of about 0.7 GPa.

Data have been collected at the neutron time-of-flight spectrometers IN4@ILL, IN6@ILL, and at the backscattering instrument IN13@ILL, all hosted by the European neutron source Institut Laue Langevin in Grenoble, France. IN6@ILL and IN13@ILL were introduced in our preceding studies of dynamic properties of amorphous and crystalline ice modifications.[9,11,31,36] The thermal neutron instrument IN4@ILL was exploited for reasons of complementarity. It offers a moderate energy resolution but an extensive coverage of the $\hbar\omega - Q$ phase space. An elastic Q range matching the one of the IN13@ILL spectrometer was accessed with the applied setup. Figure 1 reports the $\hbar\omega - Q$ phase space covered by these instruments with the incident neutron wavelengths of 2.20 Å (IN4@ILL), 4.14 Å (IN6@ILL), and 2.23 Å (IN13@ILL).

IN6@ILL was operated in the inelastic time-focusing mode in which, at the expense of the neutron flux, the resolution is improved drastically in the energy range of interest. Inelastic focusing was set to 8 meV and the resulting energy resolution in the energy range of phonons is indicated in the right plot of Fig. 1. The resolution of IN4@ILL was 0.8 meV at the elastic line $\hbar\omega = 0$.

The benefit of the IN13@ILL spectrometer for the present study is the elastic-window scan mode enabling the sampling of the Debye-Waller factor and, hence, the mean-square displacement $\langle u^2(T)\rangle$ of the molecules as a response to temperature changes.[11,36–38] Since the Debye-Waller factor relates the scattering intensity in the elastic window to the inelastic intensity, IN13@ILL monitors the properties of the vibrational

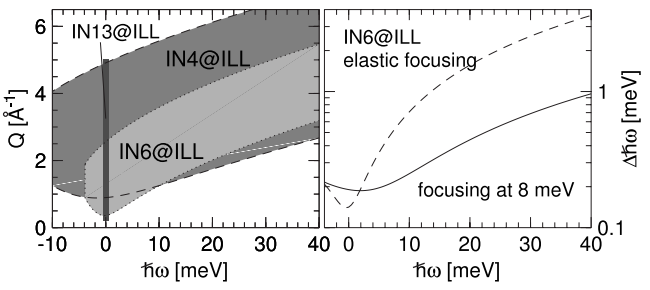

FIG. 1. Left, phase space coverage by the neutron spectrometers applied in the present study as indicated. Right, calculated resolution function of the high-resolution time-of-flight spectrometer IN6@ILL stressing the particular setup of inelastic focusing at 8 meV chosen in comparison to the standard elastic focusing working condition.

density of states, which can be measured directly at IN4@ILL within equivalent elastic Q range, as an effect on the elastic intensity. Changes to the dynamics are visualized via the elastic structure factor $S(Q,\omega=0)$ with a resolution of 8 μeV, hence, improved by about two orders of magnitude. The precision and merits of this elastic-window scan technique was demonstrated in Refs. 11 and 39 in which the recrystallization temperature of LDA into the crystalline cubic modification ice I_c was established at 135 K for deuterated samples.

The entire set of experiments on amorphous samples at the time-of-flight instruments comprised different temperatures in the range of 2–130 K, whereby 130 K was applied to each sample for 30 min only to obtain reference LDA structures. All the as-prepared and LDA structures were measured at 75 K for best statistics. Data taken at any other temperatures below showed the trivial dependence of Bose-Einstein statistics expected for harmonic phonon systems. For reasons of clarity we focus therefore on a subset of our data in the present manuscript. Details of the temperature scans used in IN13@ILL experiments are presented with the data. Results of crystalline samples could be obtained at 120 K for ice IX and V, and at 100 K for ice XII due to their higher transition temperatures into ice I_c.[36,40–42] Note that measurements have been performed as well on other spectrometers and with other samples, however, with no additional information and no deviation from the results than forwarded here.

Data treatment has been performed in analogy to the data processing discussed in detail in Refs. 11, 31, and 36. The normalization of the generalized density of states $G(\omega)$ computed from IN4@ILL and IN6@ILL data has been performed to 12 modes in the energy range 0.5–40 meV. However, please note that for the structures of highest density the librational mode intensity is apparently superimposed with the phonon signal above 34 meV. For these reasons the very high density data were normalized in respect to HDA $G(\omega)$ in the range of 0.5–30 meV. This is well justified as throughout all the studied high-density structures their density of states is homogeneously distributed with no distinguished texture in the range of 15–40 meV. Moreover, a normalization of the LDA reference data to equal intensity showed only a scatter of 2%–3% from the applied normalization.

III. RESULTS

A. Coherent signal and time-of-flight spectroscopy

The use of deuterated sample material for the core of our experiments has been considered mandatory. As we have presented in a recent paper the phonon density of states of amorphous structures require an unequivocal experimental identification and discrimination from the phonon properties of high-density crystalline phases, in particular from the one of ice XII.[36] This is best done by monitoring static correlations of the sample material via the coherent scattering from deuterated samples. Since all utilized spectrometers map out the $\hbar\omega-Q$ phase space simultaneously, they offer a direct access to the static structure factor, i.e., the observable in diffraction experiments, by appropriate data processing $S(2\Theta)=\int S(2\Theta,\omega)\cdot d\omega$. The scattering angle 2Θ can be further converted into Q via the Bragg relation.[37,38] $S(Q)$ data will be presented in the subsequent paragraphs.

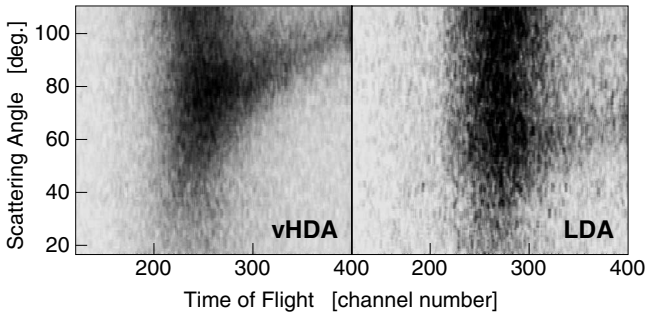

FIG. 2. Contrast plot of vHDA (left) and LDA (right) inelastic response monitored at the time-of-flight spectrometer IN6@ILL. Time-of-flight channel number and scattering angle are chosen as natural units of the measurement for presentation. The strong elastic intensity is centered around time-of-flight channel 424 and suppressed here for clarity reasons. Time channel width corresponds to 5.875 microseconds.

A coherently scattering sample offers as well the opportunity of monitoring phase coherence properties within the inelastic channels. Figure 2 reports this intensity for sample 5 in the vHDA and LDA structures. The elastic window has been suppressed for a distinct presentation of the inelastic response since the elastic intensity exceeds the inelastic one typically by 2–3 orders of magnitude. The pronounced intensity between time-of-flight channels 200 and 300 corresponds to the strong maximum in $G(\omega)$ at 7–10 meV, which is reported below. The dispersive line between channels 300 and 400 corresponds to the acoustic phonons of the two structures within the 2nd pseudo-Brillouin zone. Note that the points of origin of acoustic phonons (Γ point) in higher order Brillouin zones are the Bragg peaks in crystalline samples and the intense peaks in amorphous material. The downshift of the dispersing acoustic branch from vHDA to LDA reflects the shift of the strong peak toward smaller 2Θ and, hence, Q numbers upon the structural transformation.[32,43]

B. Vibrational density of states

Figure 3 reports the static structure factor $S(Q)$ of the samples studied and the $G(\omega)$ of the very high-density samples.

The results of samples 4 and 8 taken at IN6@ILL and IN4@ILL, respectively, are compared directly. Despite the pronounced resolution difference, factor 4–5, between these spectrometers and the different phase space mapped out, all features are well reproduced in both runs. This indicates that the smooth and untextured $G(\omega)$ profiles of the studied samples are not resolution-limited effects of the experiment. It is well established that the intensity at energies below about 40 meV stems from eigenmodes of translational character (phonons), which are characterized by displacements of the entire water molecule from its center of mass. Therefore we may safely state that no distinguished mode peaks or gaps are present in the phonon density of states of high-

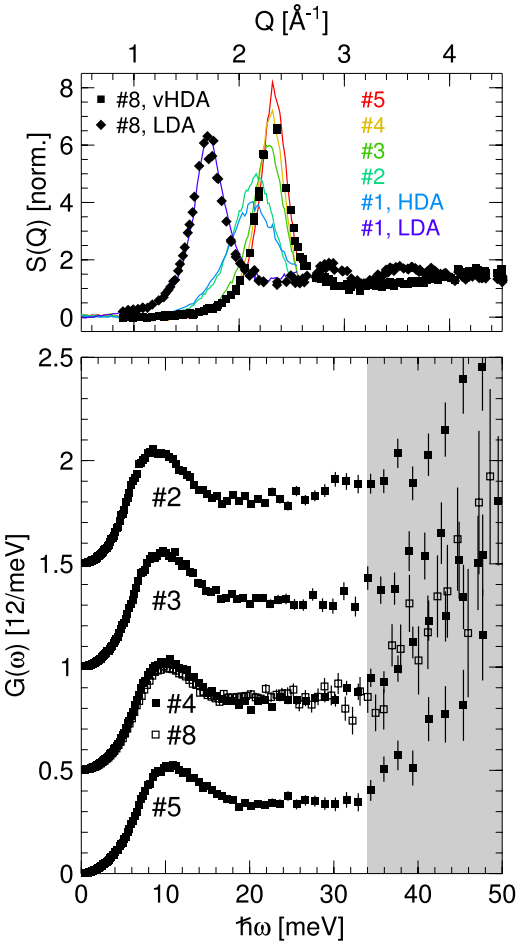

FIG. 3. (Color online) Static structure factors $S(Q)$ and generalized density of states $G(\omega)$ of very high-density amorphous structures as it is indicated in the figure. Samples 1–5 are studied at IN6@ILL with λ_i=4.14 Å, sample 8 is measured at IN4@ILL with λ_i=2.2 Å. Gray shaded area marks the energy range in which the onset of librational mode intensity in sample 5 is observed. Except for 5 all data sets are shifted for clarity.

density amorphous structures. The accuracy of this statement is given by the resolution function of the IN6@ILL setup plotted in Fig. 1 and will be stressed later on by the results on crystalline samples.

Another obvious feature of the very-high-density amorphous structures is the excess of intensity at energies above about 34 meV. This high-energy mode band is associated with librational degrees of freedom whose eigenfrequency depends on the moment of inertia of the water molecule.[44,45] It is therefore highly sensitive to the density of the sample and to the sample material, deuterated or protonated. Higher densities, as well as augmented moments of inertia, shift the librational band toward lower energies. There is some indication in the present data that the onset of librational intensity is shifted progressively from about 34 meV in sample 5 to 40 meV in sample 2 and HDA structures,[9] i.e., with decreasing density of the material. At least in the case of sample 5 translational and librational bands apparently overlap and a clear assignment of translational and librational eigenmodes is *a priori* not possible on pure experimental

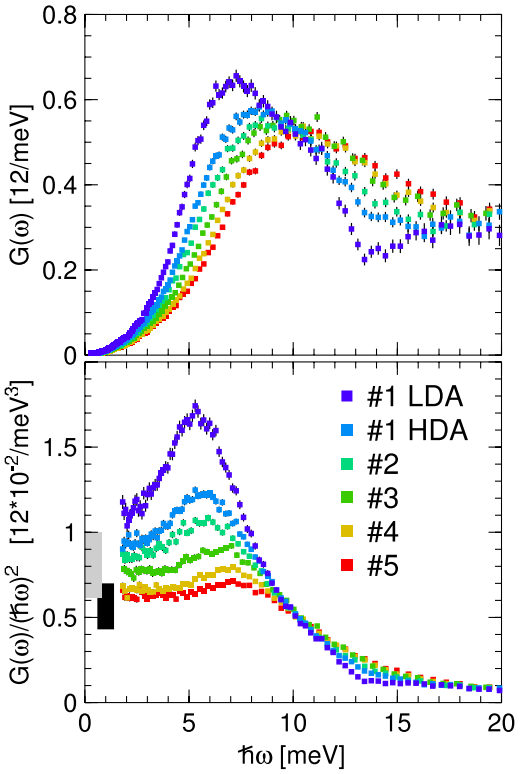

FIG. 4. (Color online) Generalized density of states $G(\omega)$ of different amorphous structures as it is indicated in the figure. Figure at bottom stresses the low-energy properties of the inelastic signal in a Debye plot $G(\omega)/(\hbar\omega)^2$. Black shaded area indicates the range of data computed from Debye temperatures determined at IN13@ILL and the gray shaded area indicates its extent corrected for the coherent signal.

grounds. However, we expect this ambivalence to be lifted for protonated sample material as librational modes should be shifted by about 15 meV to higher values.[8,36,46]

Figure 4 reports the low-energy part of $G(\omega)$. Experiments probing phonon dispersion properties and intensities as a consequence of phonon selection rules have shown that the intensity in this energy range is dominated by acoustic phonons with a contribution of low-energy optic phonon sheets of transverse polarization giving rise to the characteristic strong peak.[1,2,36] This peak is visibly redshifted upon decreasing the sample density from 10 meV in vHDA sample 5 to 7 meV in LDA structure. In accordance to the shift a narrowing and, hence, a concomitant intensity increase of this peak is observed as well. In agreement with prior results, only the LDA structures show a texture on the $G(\omega)$ profile.[8–10,31,46–48] Despite the restrictive intensity selection rules acting in Raman scattering experiments a comparable trend from broad, textureless inelastic features in high-density amorphous structures toward narrower, textured response in LDA and a redshift of the predominant peak have been observed.[49–51]

To finalize the presentation of $G(\omega)$ data Fig. 5 indicates the dynamics of samples 6 and 7, which were formed having followed a modified preparational path. There is a good correspondence of the data sets of sample 6 with sample 4 and of sample 7 with sample 3 in particular in the low-energy

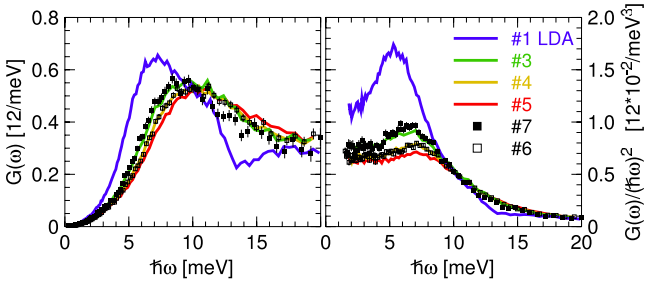

FIG. 5. (Color online) Generalized density of states $G(\omega)$ of the amorphous structures 6 and 7 compared to 4 and 3, respectively. Data on 5 and LDA are given as guide to the eye. Figure on right stresses the low-energy properties of the inelastic signal in a Debye plot $G(\omega)/(\hbar\omega)^2$.

Debye regime. However, the strong peak of sample 7 appears to be somehow narrower than the one of sample 3. Consequently, the qualitative behavior of the inelastic response of these samples reflects the behavior of the elastic signal in which an overall good match of the $S(Q)$ response has been observed with subtle deviations for example of the peak width.[32]

C. Elastic structure factor and Debye temperatures T_D

As it is shown in Figs. 4 and 5 a Debye plot $G(\omega)/(\hbar\omega)^2 \rightarrow \hbar\omega$ indicates a progressive softening of the amorphous matrix and, hence, a decrease in Debye temperatures T_D and a reduction in the average velocity of sound $\bar{v}$ passing from vHDA to LDA. Following the Debye theory of harmonic crystals[52] both quantities T_D, as well as $\bar{v}$ are linked to the density of states by

$$T_D = \left[\frac{k_B^3}{36} \cdot \frac{G(\omega)}{\hbar^2\omega^2}\right]^{-1/3}, \tag{1}$$

$$k_B \approx 8.617 \cdot 10^{-2} \text{ meV/K}, \tag{2}$$

$$\bar{v} = \left[C \cdot \frac{N}{V} \cdot \frac{G(\omega)}{\hbar^2\omega^2}\right]^{-1/3}, \tag{3}$$

and

$$C \approx 4.6905 \cdot 10^{-37} \text{ meV}^3 \text{ s}^3. \tag{4}$$

Nonetheless, due care has to be taken to the coherent signal of the samples and, as far as $\bar{v}$ is concerned to the sample density N/V, which is not known accurately.

A technique of probing T_D more accurately is given by the elastic-window scan technique of IN13@ILL. Figure 6 reports mean-square displacements $\langle u^2(T)\rangle$ obtained for samples 9 and 10. After the scan of vHDA to a temperature of 100 K sample 9 was annealed at 110 K for about 60 min. to form a structure HDA′ intermediate in respect to vHDA and LDA. Figure 6(a) reports the elastic structure factor $S(Q,\omega{=}0)$ and Fig. 6(b) the difference elastic structure factor

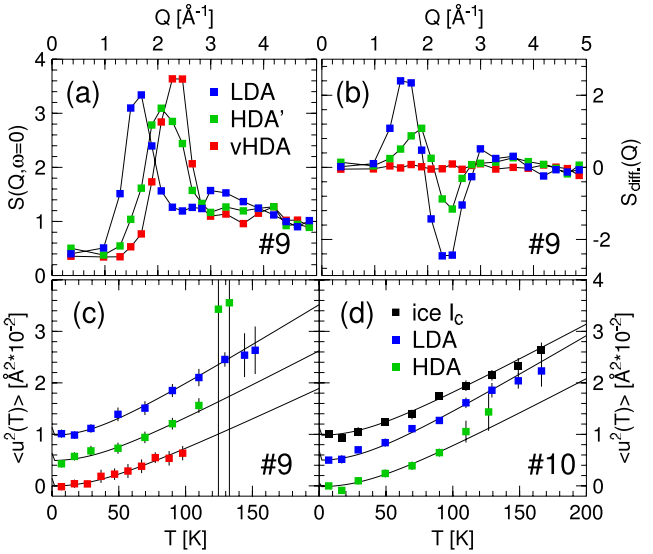

FIG. 6. (Color online) (a) Elastic structure factors $S(Q,\omega{=}0)$ of vHDA, HDA′, and LDA structures of deuterated sample 9. (b) Corresponding difference structure factors $S_{\text{diff.}}(Q)$ and (c) corresponding mean-square displacements $\langle u^2(T)\rangle$. (d) Mean-square displacements $\langle u^2(T)\rangle$ of the structures HDA, LDA, and ice I_c of protonated sample 10. Full lines with the $\langle u^2(T)\rangle$ data represent Debye fit results. $\langle u^2(T)\rangle$ and fit results of HDA′ and LDA sample 9, and of LDA and ice I_c sample 10 are shifted for clarity.

$$S_{\text{diff.}}(Q) = S_X(Q,\omega=0) - S_{\text{vHDA}}(Q,\omega=0) \tag{5}$$

of sample 9 in the three structural states X—vHDA, HDA′, and LDA, all measured at 2 K. The total intensity of the difference profiles $I = \int |S_{\text{diff.}}(Q)| \cdot \mathrm{d}Q$ indicates that HDA′ corresponds to a structure obtained when about 40% of the vHDA to LDA transformation was accomplished.

Phase transformations are manifested in the $\langle u^2(T)\rangle$ presentation shown in Fig. 6(c) and Fig. 6(d) for samples 9 and 10, respectively, by an abnormal excess of data errors and/or by an abrupt and persistent data deviation.[11,36] This way the rapid change from HDA′ to LDA and from HDA to LDA can be identified at 110–120 K in 9 and 10, respectively, and the recrystallization of LDA can be attested between 130 and 145 K in both samples.

Debye temperatures listed in Table II are obtained with Debye fits to data in the temperature range of structural stability of the samples. They are in good agreement with data obtained during extensive experiments on the HDA and LDA structures.[11,39] We may utilize the deuterated data for a consistency check with the Debye plot of Fig. 4. The range of the Debye level data when changing from vHDA to LDA is sketched by the black area. To account for the excess of intensity in the low-energy part of the data due to the coherence of the signal, we have applied the scaling argument discussed in detail in preceding papers.[11,36] The correspondence of the rescaled IN13@ILL data indicated by the light gray shaded area and the Debye levels in $G(\omega)/(\hbar\omega)^2$ is reasonably good.

D. High-density crystalline ice IX, V, and XII

The untextured profile of the $G(\omega)$ of high-density amorphous ice structures is a notable feature. To stress its signifi-

TABLE II. Debye temperature T_D and expected Debye levels $D=G(\omega)/(\hbar\omega)^2$ obtained from the present data at top and reported in Ref. 11 at bottom.

	D_2O			H_2O		
	vHDA	HDA′	LDA	HDA	LDA	ice I
T_D/K	231(10)	222(8)	203(4)	235(10)	215(6)	225(5)
D/meV^{-3}	0.46(3)	0.51(3)	0.67(2)	0.43(3)	0.57(3)	0.49(2)
T_D/K		223(9)[a]	202(3)	230(6)	217(2)	224(7)
D/meV^{-3}		0.51(4)	0.68(2)	0.46(2)	0.551(9)	0.50(3)

[a]As-prepared HDA reported in Ref. 11.

cance and the accuracy of the measurement Fig. 7 reports the inelastic response of crystalline ice IX, V, and XII samples in comparison to sample 5. They may be considered as a pictorial reference for the quality and reliability of the presented $G(\omega)$ of the amorphous structures. A more detailed presentation of ice XII dynamics is given in Ref. 36.

At the top part in Fig. 7 the static structure factor $S(Q)$ of the three deuterated crystalline samples is shown. Left column indicates the respective $G(\omega)$ in the entire range of phonons up to the edge of the librational bands. All features identified in this range are in very good agreement with data reported elsewhere.[46] The presentation in the right column focuses on the acoustic region stressing its detailed response.

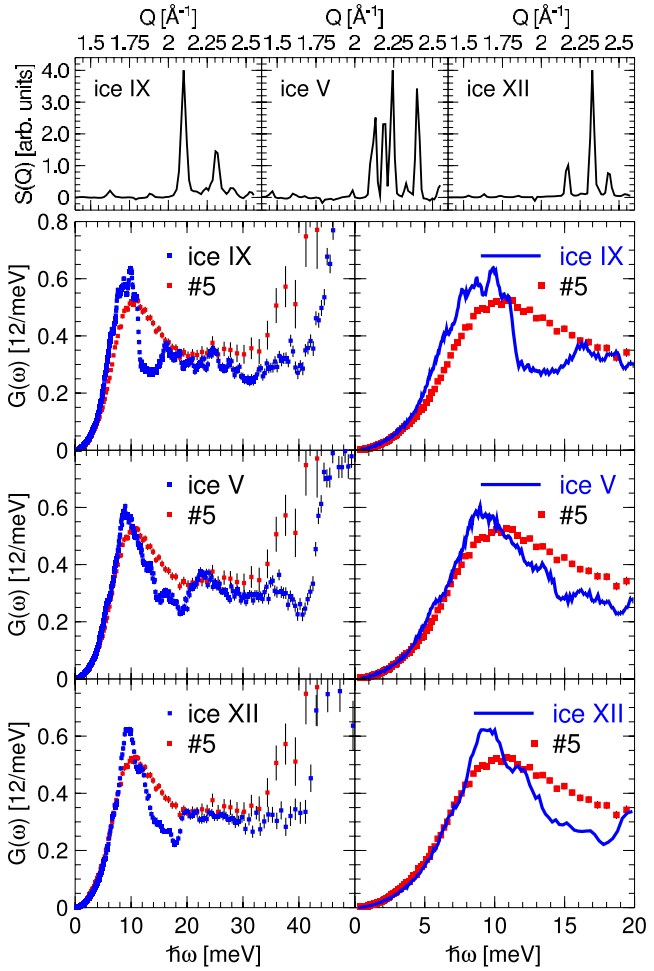

FIG. 7. (Color online) Generalized vibrational density of states $G(\omega)$ of different crystalline structures as it is indicated in the figure. On top the static structure factor $S(Q)$ of the samples are shown. Left column reports the $G(\omega)$ in the entire range of phonon modes. Right column presents the low-energy region of the spectra. The vHDA sample 5 is plotted for comparison.

Note, for example, the many fold of peaks resolved in $G(\omega)$ of ice IX and the distinguished shoulders at the low-energy flank of the predominant peak at about 10 meV in all samples. Other characteristic features of the crystalline phases are intensity gaps in their $G(\omega)$ separating the predominant peak from the higher energy phonon part. They are detectable at 12–16 meV in ice IX, 14–21 meV in ice V, and 13–20 meV in ice XII, whereby, dynamics of ice V and XII are marked by an additional pronounced mode gap at 19 and 18 meV, respectively. Such details are absent in the inelastic response of the high-density amorphous samples.

Peaks and shoulders in $G(\omega)$ are due to van Hove singularities of phonon sheets at which the group velocity $v_g = d\omega(Q)/dQ \approx 0$ at some point of the phase space.[37,38,52] Some of them are due to Brillouin zone center Γ modes, which can be Raman or infrared active.[53–55] We have therefore indicated the energy positions of these peaks and shoulders in Table III.

There are two interesting features which are worth being noted from the crystalline response. One point is the low-energy shoulder at the dominant peak of the samples whose energy is marked by an asterisk in Table III. This peak can be interpreted as due to a van Hove singularity of acoustic phonon sheets of transverse polarization in some direction of the crystal. It is apparently lowest in energy in ice V although Brillouin scattering experiments indicate an average velocity of sound of ice V higher than the one of ice III/IX.[56–58]

The other notable point is the progressive loss of defined modes in the optic phonon region of the spectra ($\hbar\omega > 20$ meV) upon density increase in the sequence of the polycrystals. In fact, this feature is clearer worked out by the inelastic incoherent experiments presented for example in Refs. 46 and 59 for ice IX and V and in Ref. 36 for ice XII. To a certain degree there is resemblance of the optic phonon response of ice XII and the high-density amorphous structures not unlike it has been reported for Raman scattering signals.[51]

E. Collective modes and phase coherence

According to the concept of translational dynamics of glasses introduced in Refs. 60–62 the collective aspect of

TABLE III. Dynamic characteristics in microelectronvolt evoked by van Hove singularities detected in the responses of the crystalline modifications ice IX, V, and XII.

ice IX													
6.5*	7.6	8.4	8.7	9.0	9.9	11.0	16.3	18.5	21	22.5	25	27.5	29
ice V													
5.8*	7.4	8.5	9.8	13.5	16	18	21	22.5	36				
ice XII													
7.0*	9.0	10	12	17	20								

acoustic phonon modes should be manifested in the coherence properties and, hence, in the form factor of the inelastic response. In a simplified picture, disorder is supposed to perturb the collective motion of the water molecules and reduce their coherence aspect in the scattering signal. In such a scenario a quasi-incoherent signal $S_{\mathrm{qinc}}(Q,\omega)\approx B(\omega)\cdot Q^2$ is evoked on the expense of the coherent contribution $S_{\mathrm{coh}}(Q,\omega)\approx A(\omega)\cdot S(Q)\cdot Q^2$ due to the destruction of phase coherence. $A(\omega)$ and $B(\omega)$ are related to the spectral density and the Debye-Waller factor of the scatterers. The suppression of any $S(Q)$ signature within the inelastic $S(Q,\omega)$ signal is supposed to mark the breakdown of collective dynamics in the benefit of localized vibrations.

The dynamic structure factor $S'(Q,\omega)$ of sample 8 in the vHDA and LDA structure is reported in Fig. 8 in a constant energy presentation. Data have been scaled by the spectral density according to $S'(Q,\omega)=S(Q,\omega)/\int S(Q,\omega)\cdot \mathrm{d}Q$, which results in a suppression of the spectral density factors $A(\omega)$ and $B(\omega)$. A variation of the intensity not conforming to an incoherent signal $S'(Q,\omega)\propto Q^2$ dependence, which is indicated by the solid lines, can be followed up to the highest energy plotted. As well, a progressive suppression of the intensity modulation can be observed.

For a quantitative evaluation of an energy limit, beyond which coherence effects are apparently suppressed a fitted $F(Q)=a_\omega+b_\omega\cdot Q^2$ background signal, has been subtracted from the data sets and the remaining Q-modulated intensity has been integrated. This data evaluation process is indicated in Fig. 9. On the right hand side the difference signal $S'(Q,\omega)-F(Q)$ of the LDA structure is reported for three selected data sets. On the left hand side the integrated signal is reported scaled for simplicity to unity value for the low-energy data (2–5 meV) of LDA.

The dominating feature in both data sets is the constant plateau up to energies of 8–10 meV and the rapid drop off onto another plateau of about null value starting at 15–16 meV. Hence, an apparent reduction of collectivity starts close to the position of the low-energy optic modes of transverse polarization and proceeds diminishing the signal coherence across the energy range of the strong maximum in $G(\omega)$ (Fig. 4). This behavior is grossly sketched in the figure by solid lines.

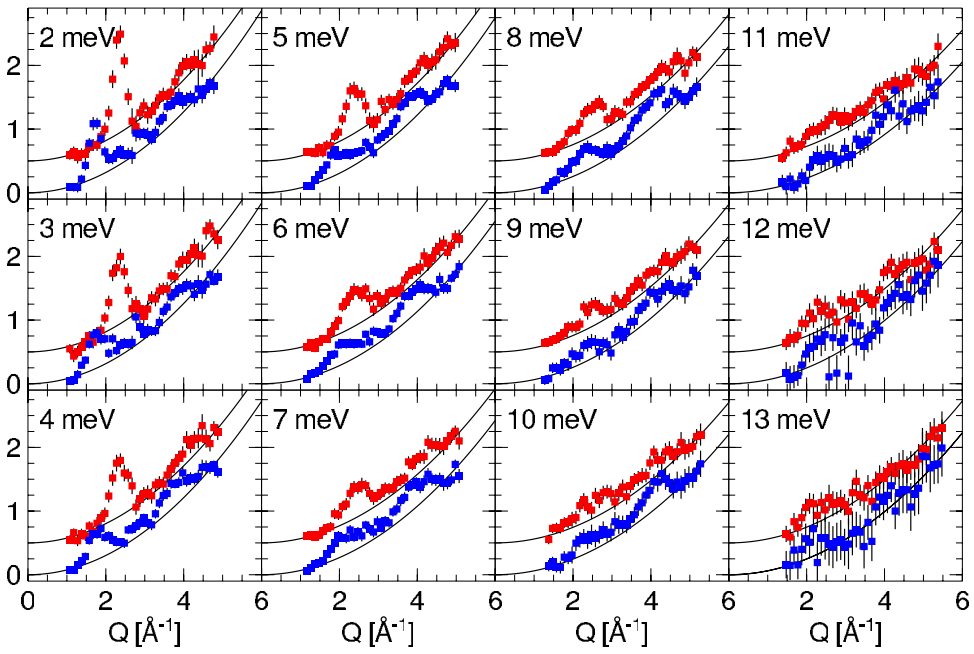

FIG. 8. (Color online) Dynamic structure factor $S'(Q,\omega)$ in a constant energy presentation measured at IN4@ILL. Energy values are given in the figures. Full lines correspond to an $a_\omega+b_\omega\cdot Q^2$ fit of the (quasi-)incoherent signal and background contribution. Data sets and fits are shifted to match $a_\omega=0$ and 0.5 for LDA (blue squares) and vHDA (red squares), respectively.

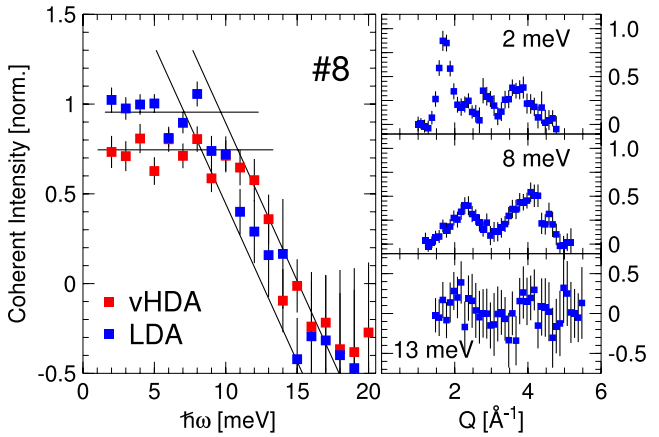

FIG. 9. (Color online) Left, coherent intensity of vHDA and LDA as indicated in the figure. See text for details. Right, bulk coherent signal of LDA after subtraction of (quasi-)incoherent signal and background contribution $F(Q)=a_\omega+b_\omega\cdot Q^2$ at the indicated energies.

Note that the data are featured by some characteristics. These characteristics are the deviation of the low-energy vHDA plateau by about 25% from the value determined for LDA, and the trend of the high-energy plateaus toward values lower than null, despite the elevated error bars. We show in Sec. IV that these effects and the loss of coherence signal can be understood within a simple scenario of acoustic phonons in a disordered structure.

Figure 10 reports on the dynamic structure factor $S'(2\Theta,\omega)$ of the samples measured at IN6. As the Q range of the high-resolution experiment is too narrow for a proper background fit with $F(Q)$, we aim here at a qualitative comparison only, and the x axis of the data is kept in natural units of the experiment, i.e., the scattering angle 2Θ. In analogy to the data of Fig. 8 a modulation of the inelastic signal reminiscent of the elastic line at $\hbar\omega=0$ meV can be unequivocally followed up to an energy of 10 meV. This modulation ceases to be obvious at about 14 meV corresponding well with the limit evaluated in Fig. 9. Within the quality of the data the limit of ceasing phase coherence shows universal validity independent of the density and structure of the samples.

IV. DISCUSSION

The particularly remarkable feature of the dynamics of high-density amorphous ice structures is the smooth profile of the generalized vibrational density of states $G(\omega)$ in the energy range of translational excitations at $\hbar\omega\lesssim 40$ meV. Except for a pronounced broad peak in the range 7–10 meV, whose intensity is reported to be dominated by optic modes, the inelastic response appears to be untextured. Density variation causes a systematic and continuous variation of features in $G(\omega)$ as it is evidenced in Figs. 3–5. $G(\omega)$ of the highest density structure 5 is characterized by a wide, textureless peak centered at about 10 meV. Upon density decrease, this peak shifts toward lower energy and takes on the minimum value of about 7 meV in the LDA structure. It is progressively narrowed and featured in the LDA structure by a texture reminiscent of the $G(\omega)$ properties of crystalline ice I_c and ice I_h.[8–10] Concomitantly, the low-energy edge of the librational band is shifted from about 34 to 45 meV (LDA) in the deuterated samples.

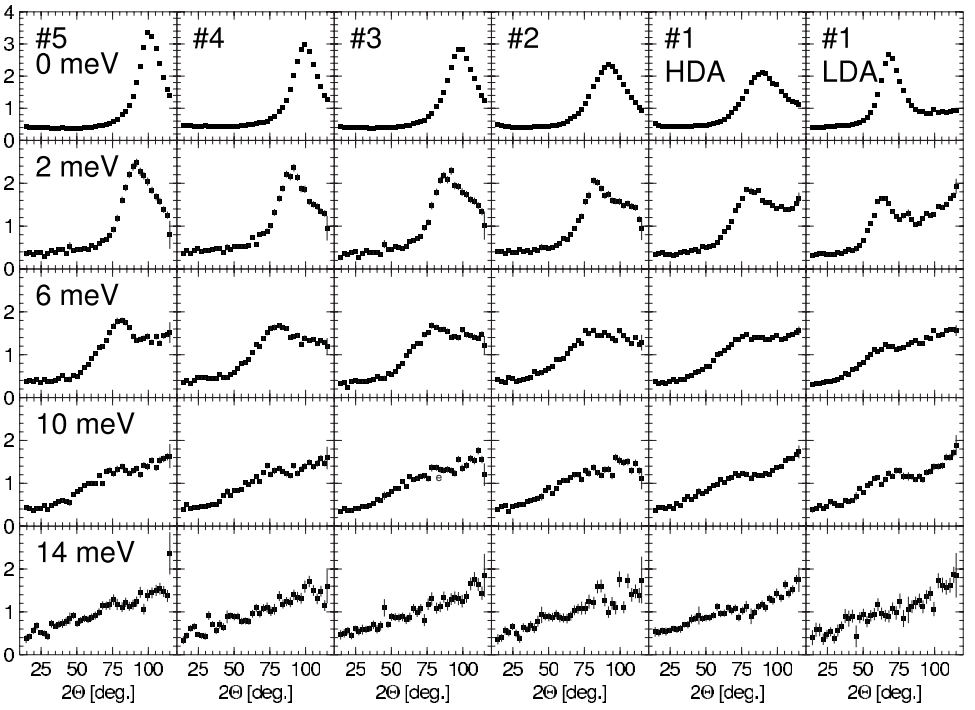

FIG. 10. Dynamic structure factor $S'(2\Theta,\omega)$ in a constant energy presentation extracted from high-resolution experiments performed at IN6@ILL. Each column of data represents selected energy slices of the samples indicated in the top figure. Energy values valid for each of the data lines are indicated in the left figures.

The overall trend of the first peak in $G(\omega)$ and of the librational band upon density changes may be expected as they have been well established as a general feature in the dynamics of crystalline counterparts.[46] It is therefore a generic behavior of ice modifications. The textureless profile of $G(\omega)$ is, however, the more remarkable as amorphous ice structures proved to show in IXS experiments the sharpest phonon excitations of disordered samples so far measured.[1,2] As a consequence, an analogy of $G(\omega)$ of high-density amorphous ice modifications and of liquid water might be apparent,[50,63] however, CINS and IXS experiments probing the dynamic structure factor $S(Q,\omega)$ give evidence of a markedly distinct behavior of the collective excitations,[64–66] questioning the justification of a substantial comparison of phonon properties of the solid amorphous with the liquid phase. Moreover, even within the experimental reports of spectral density data a link between the liquid and solid amorphous structures is questioned.[67,68]

The untextured response of $G(\omega)$ has to be particularly stressed as our data are at contrast to data sets published in the literature trying to comment on the inelastic response of amorphous ice structures.[46,48,69–71] Our prior study of the ice XII dynamics constitutes a first approach on trying to scrutinize this contrast and reports in detail on the experimental procedure required when purely incoherent inelastic neutron scattering is involved.[36]

It has been recently demonstrated that the redshift and narrowing of the pronounced low-energy peak in $G(\omega)$ is not a property of the as-prepared high-density structures. It can be well reproduced by following the evolution of the amorphous matrix during the temperature induced transformation of some high-density amorphous modification into LDA.[31] Consequently, $G(\omega)$ reflects in an equivalent way the changes and properties of the static structure factor.[9,31,32,34,43,72] The wide-angle diffraction response $S(Q)$ of the amorphous structures follows a systematic and continuous variation, which reflects the microscopic density of the sample as the position of the first peak in $S(Q)$ and the homogeneity of the sample as the width of this peak. This feature can be concluded from the $S(Q)$ data in Fig. 3 taking into account that the density of the structures is progressively reduced in the inverse sequence 5–1 (LDA).

It has been as well shown that there are only two structures which can be termed homogeneous,[31] namely the structures of highest and lowest density, i.e., vHDA (here sample 5) and LDA. Intermediate amorphous structures comprising HDA′ and the as-prepared HDA are of heterogeneous nature and, hence, structural mixtures of some kind.[9,31–34,73] This heterogeneity is apparently not reflected in the presented inelastic data, a statement not only applicable to the density of states but also to the extent of phase coherence, as it is discussed in Sec. III E. However, the validity of this statement is hampered and limited by the accuracy and significance of the data treatment procedure. Whereas this accuracy is high for the obtained $G(\omega)$ it is relaxed for the phase coherence discussion. The obstacle of a reliable separation of the incoherent and/or quasi-incoherent signal from the coherent one and the sampling of the inelastic response in the second and higher pseudo-Brillouin zones[1,2,36] reduce the significance of the extracted phase coherent intensity in Fig. 9. The approximated value of 15 meV for the energy of apparently ceasing phase coherence should be seen as a lower limit of the real extent of phase coherence.

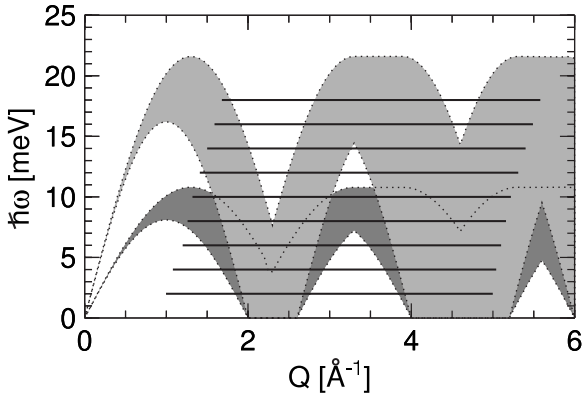

FIG. 11. Dispersion of acoustic phonons of transverse (v_t =2000 m/s) and longitudinal characteristics (v_l=4000 m/s) in a structure with ill-defined translational symmetry. Horizontal lines indicate the Q sampling by the IN4@ILL experiment whose spectra are reported in Fig. 8.

We wish to substantiate this statement with a very simple but instructive scenario of acoustic phonons in a disordered sample. Figure 11 reports the phase space as it has been approximately accessed on IN4@ILL and horizontal lines indicate the constant energy slices as they have been shown in Fig. 8. Dark and light gray shaded areas correspond with averaged acoustic phonon dispersions of transverse and longitudinal character, respectively. They have been calculated following two simple assumptions: (1) Any transverse acoustic phonon propagates with the velocity of sound v_t =2000 m/s and any longitudinal one with v_l=4000 m/s, i.e., in good approximation to the values of polycrystalline ice, and as we will show in a proceeding study, as well as to the velocities of sound of vHDA. (2) The translational symmetry is ill–defined allowing for a variation of the symmetry center between 2.0 and 2.6 $Å^{-1}$, hence, with an average value 2.3 $Å^{-1}$ matching the approximative spatial correlation in very high-density amorphous ice (vHDA).

It is immediately obvious from this presentation that we expect to loose phase coherent signal from about 8–10 meV on due to the progressive loss of intensity by transverse acoustic phonons (dark shaded area). The extent of the spectra shows that the fit $F(Q)$ to the background, as it was performed, overestimates the (quasi-)incoherent contribution, since it is matched to potentially coherent signal in particular at the high Q limit of the spectra. Consequently, this very simple scenario offers an intuitive explanation to the coherence loss above 10 meV and the trend toward negative values of the extracted coherent intensity of Fig. 9.

The strong variations of symmetry centers and velocities of sound with different amorphous structures alter the sketched acoustic phonon scenario, accordingly. Therefore, the reliability of the incoherent and quasi-incoherent background estimation varies and causes, for example, the departure of the low-energy vHDA value in Fig. 9 from unity when normalized to the numbers of LDA.

The reliability of the $G(\omega)$ features is not only established by the simultaneously monitored structure factor $S(Q)$ of the

samples in the coherent inelastic neutron scattering (CINS) experiments. A cross check with observables reported in the literature shows a good correspondence of properties determined by the Debye level of the density of states. This holds for a direct comparison of the $G(\omega)$ obtained from neutron scattering experiments,[8,10] it can be conjectured from properties of the inelastic signal in Raman scattering experiments,[49–51] as well as from properties linked to the phonon system such as the velocity of sound,[14,15] Grueneisen–parameters,[18] and thermal conductivity.[16,17,28] In this respect the Debye-Waller factors, mean-square displacements, and, hence, Debye temperatures T_D obtained from the backscattering experiments are of particular virtue, since they are sampled with high accuracy and are not subject to normalization procedures except the one to the low-temperature measurements canceling out zero-point oscillations. Throughout all of our measurements the computed T_D correspond well with the Debye levels $G(\omega)/(\hbar\omega)^2$ computed from the time-of-flight experiments. This applies to the amorphous systems, as well as to the crystalline modifications ice I_h, I_c, and XII.[11,36]

Both techniques—neutron time–of–flight and backscattering spectroscopy—exclude the presence of an excess signal in the low-energy part of the spectra, often referred to as boson peak. There is a substantial discussion in the amorphous ice literature about the existence of such a low-energy dynamic feature. Experimental approaches identified this transient low-energy feature in the as-prepared HDA inelastic response, which does not follow the Bose-Einstein statistics of a phonon system.[74–78] The excess signal being subject to saturation effect by temperature increase has been conjectured to be due to the presence of two-level systems. As we have outlined in a prior publication[11] this experimentally established inelastic feature is not in contrast with our inelastic neutron scattering data. However, it is in contrast with an excess of vibrational modes of boson type, i.e., with a boson peak. A simple mode excess due to lattice dynamics[79,80] cannot be brought in agreement with our results of $G(\omega)$ and in particular of the Debye temperatures T_D. It is as well at contrast to the results from supersonic experiments probing the velocity of sound and material constants of amorphous and crystalline structures.[14,15]

As far as the as-prepared HDA structure is concerned, it has been shown by inelastic x-ray scattering (IXS) experiments that its longitudinal velocity of sound v_l is indeed reduced in comparison to crystalline ice I_c and I_h.[1,2,81] This finding is in excellent agreement with results from the supersonic experiments. The smaller v_l is, however, counter balanced in the density of states data $G(\omega)$ by a higher transverse velocity of sound v_t (Ref. 14) and in particular by the higher molecular density N/V of the amorphous sample [Eq. (4)]. In fact, all T_D determined for HDA in our experiments show the trend to be augmented over the crystalline counterpart values. This counter balance effect by the sample density is lifted for the LDA structure[9–11] and its higher $G(\omega)/(\hbar\omega)^2$ value is an effect of the softer matrix leading to smaller T_D.

When taking into account the deuteration effect on the T_D the as-prepared vHDA, e.g., sample 5, indicates a T_D close to the one of ice XII of about 340 K.[36] The deuteration effect is due to the higher mass M of the D_2O molecule taking influence on the energy scale of $G(\omega)$ by $\omega \propto 1/\sqrt{M}$. Within the HDA, LDA, and ice I_c backscattering data it is observed as a reduction of T_D (Table II) by 10–15 K.[11,36]

Despite the contrast upon the low-energy properties of $G(\omega)$ the overall behavior of the simulated data in Refs. 80 and 82, as well as Refs. 83–85, corresponds reasonably well with the results obtained experimentally. This applies to the textureless profile of the high-density amorphous response, to the redshift of the pronounced peak below 10 meV upon density decrease and to the concomitant hardening of the librational band.

The presence of acoustic phonons up to energies of about 15 meV indicated by the phase modulated spectra $S(Q,\omega)$ (Figs. 7 and 8) is not an unexpected feature of the amorphous ice dynamics. It is rather in agreement with prior CINS and IXS experiments on amorphous and on crystalline ice structures. In the case of experiments on single crystal and polycrystalline ice I_h and I_c samples,[1,65,86,87] a longitudinal acoustic phonon whose eigenvector can be followed to energies exceeding 20 meV is reported. A comparable behavior has been attested for the dynamics of the high-density polycrystal ice XII.[36] The phase coherence detected in the different amorphous structures is therefore a remnant of the crystalline ice dynamics. As for crystalline samples the CINS signal is detected via umklapp scattering processes of acoustic phonons $\vec{Q}=\vec{G}_{\mathrm{hkl}}\pm\vec{q}$, which are directly detectable at low $\vec{Q}=\vec{q}$ numbers by IXS. We conjecture that the rather well-defined phase coherence of the amorphous signal up to 8–10 meV in the second pseudo-Brillouin zone reflects the crystal–like dynamics of the direct process within the first pseudo-Brillouin zone sampled by IXS. Both signals—the one obtained via the direct process, as well as the one obtained via umklapp scattering—are visibly unaffected by any hypothetical boson peak.

Let us finish the discussion with the obvious question whether the presented dynamic response can assist any of the structure models for LDA, HDA, vHDA, and other supposedly distinguished amorphous structures that have been discussed in the literature. It is of importance to stress that in all our spectroscopic studies be it on the transformation of HDA to LDA, vHDA to LDA, or some annealed HDA and vHDA structures the inelastic response showed a continuous variation and evolution.[9,31] We could not establish any distinct dynamic features, which would mark one or some of the intermediate and/or annealed structures as particular "states." To be specific, the significance of some "expanded" HDA[88,89] cannot be confirmed by the CINS and IXS results. Neither can be found a signature accentuating a particular local molecular configuration in HDA as it is conjectured from modeling diffraction data of LDA, HDA, and vHDA.[90,91]

The observation of a progressive reduction of defined inelastic features upon density increase could be understood as being in qualitative agreement with the conclusions presented in the pioneering diffraction works on LDA and HDA.[63,92,93] They explain the structure of the high-density amorphous sample as a deformed fully bonded water network with progressively distorted O–O–O bond angles with

respect to the tetrahedral coordination established on a local scale in LDA. The extremely textureless density of states $G(\omega)$ of vHDA might be understood in this context as due to bond angle distortions more pronounced than in HDA. However, without a successful and comprehensive modeling of the inelastic response of the different amorphous modifications the validity of such a conclusion is elusive.

For this very reason, we wish the inelastic neutron scattering data presented here and in prior publications to be understood as additional and complementary information to diffraction data and to results from other spectroscopic techniques. Since the vibrational dynamics is governed by the force constant distribution, hence, the second derivative of the atomic potentials, it is a highly sensitive probe of molecular arrangements present in a sample. We hope that the extraordinary dynamic features of the amorphous water ice structures detected by IXS and CINS will find its application and offer some help for cross checking of computer-generated amorphous water structures.

V. SUMMARY AND CONCLUSIONS

In the present study we have determined the generalized vibrational density of states $G(\omega)$ of amorphous ice structures of different density on samples prepared from deuterated material. We have established characteristic dynamic features in $G(\omega)$, which are a pronounced peak in the range of 7–10 meV, a textureless profile in the entire energy range of translational excitations $\hbar\omega \lesssim 40$ meV and a librational band edge at energies as low as 34 meV in the highest density structure measured. A redshift of the low-energy peak from 10 to 7 meV, its concomitant narrowing, and a hardening of the librational band from 34 to 45 meV has been observed upon reducing the density of the amorphous sample from about 41 molec./nm^3 in vHDA to 31 molec./nm^3 in LDA. The structureless profile of $G(\omega)$ was emphasized by the comparison to data obtained on the high-density crystalline structures ice IX, V, and XII.

No pronounced excess of modes in the low-energy region of $G(\omega)$ was observed. This finding was cross checked by the determination of Debye temperatures T_D via the sampling of the Debye-Waller factor. Both experimental approaches, the direct determination of $G(\omega)$, of the Debye level $G(\omega)/(\hbar\omega)^2$ and, hence, of T_D, on one hand, and its determination by sampling of the Debye-Waller factor, on the other hand, supply values in agreement with experimental data reported in the literature. A detailed comparison and discussion of the experimental results with simulated data has been given

Having followed the glass idea of reduced phase coherence in the presence of disorder we could establish correlated and collective modes up to energies of at least 15 meV. This finding was independent from the amorphous structure and its density, i.e., vHDA, HDA, or LDA.

ACKNOWLEDGMENTS

The author thanks Mark Robert Johnson and Helmut Schober for fruitful and instructive discussions and the ILL College 6 subcommittee for the support of this extensive work and the grant of accessing the instruments of the European neutron source Institut Laue Langevin. Louis Melesi and Jean–Luc Laborier are thanked for their technical support with high-pressure sample preparation equipment and Stephen Jenkins for general technical advice and help. The access to IN13@ILL for a test beam time granted by Judith Peters and Francesca Natali is very much appreciated.

*koza@ill.fr

[1] H. Schober, M. M. Koza, A. Tolle, C. Masciovecchio, F. Sette, and F. Fujara, Phys. Rev. Lett. **85**, 4100 (2000).
[2] M. M. Koza, H. Schober, B. Geil, M. Lorenzen, and H. Requardt, Phys. Rev. B **69**, 024204 (2004).
[3] O. Mishima, L. D. Calvert, and E. Whalley, Nature (London) **310**, 393 (1984).
[4] A. K. Garg, Phys. Status Solidi A **110**, 467 (1988).
[5] J. D. Londono, W. Kuhs, and J. L. Finney, J. Chem. Phys. **98**, 4878 (1993).
[6] C. Lobban, J. L. Finney, and W. F. Kuhs, Nature (London) **391**, 268 (1998).
[7] M. O'Keeffe, Nature (London) **392**, 879 (1998).
[8] D. D. Klug, E. Whalley, E. C. Svensson, J. H. Root, and V. F. Sears, Phys. Rev. B **44**, 841 (1991).
[9] H. Schober, M. M. Koza, A. Toelle, F. Fujara, C. A. Angell, and R. Boehmer, Physica B (Amsterdam) **241-243**, 897 (1998).
[10] O. Yamamuro, Y. Madokoro, H. Yamasaki, T. Matsuo, I. Tsukushi, and K. Takeda, J. Chem. Phys. **115**, 9808 (2001).
[11] M. M. Koza, B. Geil, H. Schober, and F. Natali, Phys. Chem. Chem. Phys. **7**, 1423 (2005).
[12] A. P. Sokolov, R. Calemczuk, B. Salce, A. Kisliuk, D. Quitmann, and E. Duval, Phys. Rev. Lett. **78**, 2405 (1997).
[13] C. A. Angell, Annu. Rev. Phys. Chem. **55**, 559 (2004).
[14] E. L. Gromnitskaya, O. V. Stal'gorova, V. V. Brazhkin, and A. G. Lyapin, Phys. Rev. B **64**, 094205 (2001).
[15] E. L. Gromnitskaya, O. V. Stal'gorova, A. G. Lyapin, V. V. Brazhkin, and O. B. Tarutin, JETP Lett. **78**, 488 (2003).
[16] O. Andersson and H. Suga, Phys. Rev. B **65**, 140201(R) (2002).
[17] O. Andersson and A. Inaba, Phys. Chem. Chem. Phys. **7**, 1441 (2005).
[18] O. Andersson and A. Inaba, J. Chem. Phys. **122**, 124710 (2005).
[19] E. L. Gromnitskaya, O. V. Stal'gorova, and V. V. Brazhkin, JETP **85**, 109 (1997).
[20] O. V. Stal'gorova, E. L. Gromnitskaya, V. V. Brazhkin, and A. G. Lyapin, JETP Lett. **69**, 694 (1999).
[21] A. G. Lyapin, O. V. Stal'gorova, E. L. Gromnitskaya, and V. V. Brazhkin, JETP **94**, 283 (2002).
[22] T. Strassle, A. M. Saitta, S. Klotz, and M. Braden, Phys. Rev. Lett. **93**, 225901 (2004).
[23] T. Strassle, S. Klotz, G. Hamel, M. M. Koza, and H. Schober, Phys. Rev. Lett. **99**, 175501 (2007).
[24] O. Mishima, Nature (London) **384**, 546 (1996).
[25] V. P. Shpakov, J. S. Tse, V. R. Belosludov, and R. V. Belosludov,

J. Phys.: Condens. Matter **9**, 5853 (1997).
[26] J. S. Tse, D. D. Klug, C. A. Tulk, J. Swainson, E. C. Svensson, C.-K. Loong, V. Shpakov, V. R. Belosludov, R. V. Belosludov, and Y. Kawazoe, Nature (London) **400**, 647 (1999).
[27] P. G. Debenedetti, J. Phys.: Condens. Matter **15**, R1669 (2003).
[28] G. P. Johari and O. Andersson, Thermochim. Acta **461**, 14 (2007).
[29] T. Loerting, C. Salzmann, I. Kohl, E. Mayer, and A. Hallbrucker, Phys. Chem. Chem. Phys. **3**, 5355 (2001).
[30] Please note, that according to the present perception on transition properties of different amorphous ice structures (Refs. 43, 32, and 34) on the *p-T* regions of their structural stability (Refs. 24 and 29) and on the contemporary nomenclature applied in many publications, a reconsideration of the sample assignment used in prior publications is necessary in some cases, and might be as well in some others. Reference 50 is mentioned here as a clear example in which the dynamics of a sample "HDA" nowadays, however, known and referred to as vHDA has been studied.
[31] M. M. Koza, B. Geil, K. Winkel, C. Kohler, F. Czeschka, M. Scheuermann, H. Schober, and T. Hansen, Phys. Rev. Lett. **94**, 125506 (2005).
[32] M. M. Koza, T. Hansen, R. P. May, and H. Schober, J. Non-Cryst. Solids **352**, 4988 (2006).
[33] M. M. Koza, R. P. May, and H. Schober, J. Appl. Crystallogr. **40**, s517 (2007).
[34] M. M. Koza, T. Hansen, R. P. May, and H. Schober (unpublished).
[35] M. M. Koza, H. Schober, T. Hansen, A. Tolle, and F. Fujara, Phys. Rev. Lett. **84**, 4112 (2000).
[36] M. M. Koza, H. Schober, S. F. Parker, and J. Peters, Phys. Rev. B **77**, 104306 (2008).
[37] S. W. Lovesey, *Theory of Neutron Scattering from Condensed Matter* (Oxford Science, Oxford, UK, 1984).
[38] G. L. Squires, *Introduction to the Theory of Thermal Neutron Scattering* (Dover, New York, 1996).
[39] B. Geil, M. M. Koza, F. Fujara, H. Schober, and F. Natali, Phys. Chem. Chem. Phys. **6**, 677 (2004).
[40] M. Koza, H. Schober, A. Toelle, F. Fujara, and T. Hansen, Nature (London) **397**, 660 (1999).
[41] T. Hansen, M. M. Koza, and W. Kuhs, J. Phys.: Condens. Matter **20**, 285104 (2008).
[42] T. Hansen, M. M. Koza, P. Lindner, and W. Kuhs, J. Phys.: Condens. Matter **20**, 285105 (2008).
[43] M. M. Koza, H. Schober, H. E. Fischer, T. Hansen, and F. Fujara, J. Phys.: Condens. Matter **15**, 321 (2003).
[44] H. Prask, H. Boutin, and S. Yip, J. Chem. Phys. **48**, 3367 (1968).
[45] H. J. Prask, S. F. Trevino, J. D. Gault, and K. W. Logan, J. Chem. Phys. **56**, 3217 (1972).
[46] J. C. Li, J. Chem. Phys. **105**, 6733 (1996).
[47] A. I. Kolesnikov, J. C. Li, S. Dong, I. F. Bailey, R. S. Eccleston, W. Hahn, and S. F. Parker, Phys. Rev. Lett. **79**, 1869 (1997).
[48] A. I. Kolesnikov, J. Li, S. F. Parker, R. S. Eccleston, and C. K. Loong, Phys. Rev. B **59**, 3569 (1999).
[49] H. Kanno, K. Tomikawa, and O. Mishima, Chem. Phys. Lett. **293**, 412 (1998).
[50] Y. Suzuki, Y. Takasaki, Y. Tominaga, and O. Mishima, Chem. Phys. Lett. **319**, 81 (2000).
[51] Y. Yoshimura, S. T. Stewart, H. K. Mao, and R. J. Hemley, J. Chem. Phys. **126**, 174505 (2007).
[52] N. D. Ashcroft and N. W. Mermin, *Solid State Physics* (Saunders, Philadelphia, 1976).
[53] J. E. Bertie and B. F. Francis, J. Chem. Phys. **77**, 1 (1982).
[54] B. Minceva-Sukarova, W. F. Sherman, and G. R. Wilkinson, J. Phys. C **17**, 5833 (1984).
[55] C. Salzmann, I. Kohl, T. Loerting, E. Mayer, and A. Hallbrucker, J. Phys. Chem. B **106**, 1 (2002).
[56] R. E. Gagnon, H. Kiefte, M. J. Clouter, and E. Whalley, J. Phys. (Paris), Colloq. **48**, C1-23 (1987).
[57] R. E. Gagnon, H. Kiefte, and M. J. Clouter, J. Chem. Phys. **92**, 1909 (1990).
[58] C. A. Tulk, H. Kiefte, M. J. Clouter, and R. E. Gagnon, J. Phys. Chem. B **101**, 6154 (1997).
[59] J. C. Li, J. D. Londono, D. K. Ross, J. L. Finney, J. Tomkinson, and W. F. Sherman, J. Chem. Phys. **94**, 6770 (1991).
[60] J. M. Carpenter and C. A. Pelizzari, Phys. Rev. B **12**, 2391 (1975).
[61] J. M. Carpenter and C. A. Pelizzari, Phys. Rev. B **12**, 2397 (1975).
[62] U. Buchenau, Z. Phys. B: Condens. Matter **58**, 181 (1985).
[63] M.-C. Bellissent-Funel, J. Teixeira, and L. Bosio, J. Chem. Phys. **87**, 2231 (1987).
[64] F. Sette, G. Ruocco, M. Krisch, U. Bergmann, C. Masciovecchio, V. Mazzacurati, G. Signorelli, and R. Verbeni, Phys. Rev. Lett. **75**, 850 (1995).
[65] G. Ruocco, F. Sette, M. Krisch, U. Bergmann, C. Masciovecchio, and R. Verbeni, Phys. Rev. B **54**, 14892 (1996).
[66] F. Sacchetti, J.-B. Suck, C. Petrillo, and B. Dorner, Phys. Rev. E **69**, 061203 (2004).
[67] Y. Yoshimura and H. Kanno, Chem. Phys. Lett. **349**, 51 (2001).
[68] D. D. Klug, C. A. Tulk, E. C. Svensson, and C. K. Loong, Phys. Rev. Lett. **83**, 2584 (1999).
[69] A. I. Kolesnikov, V. V. Sinitsyn, E. G. Ponyatovsky, I. Natkaniec, and L. S. Smirnov, J. Phys.: Condens. Matter **6**, 375 (1994).
[70] A. I. Kolesnikov, V. V. Sinitsyn, E. G. Ponyatovsky, I. Natkaniec, L. S. Smirnov, and J. C. Li, J. Phys. Chem. B **101**, 6082 (1997).
[71] Y. Wang, A. I. Kolesnikov, S. L. Dong, and J. C. Li, Can. J. Phys. **81**, 401 (2003).
[72] C. A. Tulk, C. J. Benmore, J. Urquidi, D. D. Klug, J. Neuefeind, B. Tomberli, and P. A. Egelstaff, Science **297**, 1320 (2002).
[73] C. A. Tulk, R. Hart, D. D. Klug, C. J. Benmore, and J. Neuefeind, Phys. Rev. Lett. **97**, 115503 (2006).
[74] N. I. Agladze and A. J. Sievers, Phys. Rev. Lett. **80**, 4209 (1998).
[75] N. I. Agladze and A. J. Sievers, Europhys. Lett. **40**, 53 (2001).
[76] N. I. Agladze and A. J. Sievers, Physica B (Amsterdam) **316-317**, 513 (2002).
[77] E. C. Svensson, W. Montfrooij, V. F. Sears, and D. D. Klug, Physica B (Amsterdam) **194-196**, 409 (1994).
[78] C. A. Tulk, D. D. Klug, E. C. Svensson, V. F. Sears, and J. Katsaras, Appl. Phys. A: Mater. Sci. Process. **74**, S1185 (2002).
[79] J. S. Tse, D. D. Klug, C. A. Tulk, E. C. Svensson, I. Swainson, V. P. Shpakov, and V. R. Belosludov, Phys. Rev. Lett. **85**, 3185 (2000).
[80] O. S. Subbotin, V. R. Belosludov, T. M. Inerbaev, R. V. Belosludov, and Y. Kawazoe, Comput. Mater. Sci. **36**, 253 (2006).
[81] G. Ruocco and F. Sette, J. Phys.: Condens. Matter **11**, R259 (1999).
[82] O. S. Subbotin and V. R. Belosludov, J. Struct. Chem. **47**, S61

(2006).
[83] R. Martonak, D. Donadio, and M. Parrinello, Phys. Rev. Lett. **92**, 225702 (2004).
[84] B. Guillot and Y. Guissani, J. Chem. Phys. **119**, 11740 (2003).
[85] R. Martonak, D. Donadio, and M. Parrinello, J. Chem. Phys. **122**, 134501 (2005).
[86] B. Renker, *Physics and Chemistry of Ice* (Royal Society of Canada, Ottawa, 1973).
[87] F. Sette, G. Ruocco, M. Krisch, C. Masciovecchio, R. Verbeni, and U. Bergmann, Phys. Rev. Lett. **77**, 83 (1996).
[88] R. J. Nelmes, J. S. Loveday, T. Straessle, C. L. Bull, M. Guthrie, G. Hamel, and S. Klotz, Nat. Phys. **2**, 414 (2006).
[89] K. Winkel, M. S. Elsaesser, E. Mayer, and T. Loerting, J. Chem. Phys. **128**, 044510 (2008).
[90] J. L. Finney, A. Hallbrucker, I. Kohl, A. K. Soper, and D. T. Bowron, Phys. Rev. Lett. **88**, 225503 (2002).
[91] J. L. Finney, D. T. Bowron, A. K. Soper, T. Loerting, E. Mayer, and A. Hallbrucker, Phys. Rev. Lett. **89**, 205503 (2002).
[92] L. Bosio, G. P. Johari, and J. Teixeira, Phys. Rev. Lett. **56**, 460 (1986).
[93] A. Bizid, L. Bosio, A. Defrain, and M. Oumezzine, J. Chem. Phys. **87**, 2225 (1987).